An Integrated Approach to the Design and Analysis of Navigation, Guidance and Control Systems for AUVs *

Daniel Fryxell, Paulo Oliveira, António Pascoal and Carlos Silvestre
Institute for Systems and Robotics
Instituto Superior Técnico
Av. Rovisco Pais, 1096 Lisboa Codex, Portugal

Abstract

This paper describes an integrated approach to the design and analysis of navigation, guidance and control systems for Autonomous Underwater Vehicles (AUV's). The general framework is illustrated with a design exercise in which recent developments in multivariable control theory and classical results in navigation and guidance were applied to the design of a trajectory following system for the AUV MARIUS (Marine Utility Vehicle System).

1 Introduction

The importance of developing methods for automatic acquisition and processing of ocean data can hardly be overemphasised. The ocean is a source of minerals and a reservoir of natural gas and oil, and its living species constitute a renewable supply of protein. Furthermore, it impacts on the global climate and the environment. With current means at one's disposal, the activity of acquiring ocean data is costly and risky. For these reasons, "our understanding of the physical, chemical, geophysical and biological processes that take place in the ocean is rather limited" [2].

There is currently great interest in the potential of Autonomous Underwater Vehicles (AUVs) to substantially reduce the costs and the risk associated with the exploration of the ocean. AUVs exhibit high maneuverability, and do note require permanent support from a ship or direct control via an umbilical cord. Moreover, their operation does not jeopardize human lives directly. There are, however, concerns that the technologies required to achieve truly autonomous behaviour are "necessarily advanced and remain developmental" [2]. The long term goal of using AUVs for the exploration of the ocean requires a committed research and development effort to develop sophisticated mobile units endowed with advanced systems for *navigation, guidance* and *control*.

This paper addresses the problem of developing guidance, navigation and control systems for AUV's to achieve accurate tracking of trajectories defined in an universal reference frame. The framework adopted for its solution is illustrated with a design exercise in which recent developments in multivariable control theory and classical results in navigation and guidance were applied to the design of a trajectory following system for the AUV MARIUS (Marine Utility Vehicle System) [6, 25]. The key ideas in the design methodology are to clearly state performance specifications in the frequency domain, and to use design tools that are adequate to this type of specifications. Thus, the natural constraint that the navigation, control and guidance systems exhibit decreasing bandwidths, can be directly incorporated in the initial phase of the project. Analysis of the integrated system is performed using a simulation package that allows the user to assess the impact of the navigation, guidance, and control algorithms on the dynamic behaviour of the vehicle.

The organization of the paper reflects the sequence of steps that go into the design of a trajectory following system for an AUV.

Section 2 describes the general model for the dynamics of underwater vehicles that are propelled by thrusters and steered by deflecting surfaces. This model is the kernel of a simulator that includes the AUV rigid body dynamics, the dynamics of the thrusters, and the hydrodynamic effects of the hull and deflecting surfaces. The general model has been tuned for the MARIUS vehicle, based on hydrodynamic data obtained in tank tests at the Danish Maritime Institute, Lyngby, Denmark. The system identification procedure is described, and the expected performance of the vehicle is analysed.

Section 3 describes the design of a control system for the vehicle in the vertical plane. The selected method is gain scheduled control. The nonlinear plant model derived in Section 2 is linearized about a finite set of operating conditions, and a linear controller is designed for each linearized plant by minimizing an $\mathcal{H}_\infty$ -criterion. The resulting finite set of linear feedback controllers is then interpolated and scheduled according to forward speed (scheduling variable). A new methodology, henceforth referred to as the $\mathcal{D}$- methodology, is described to implement the gain-scheduled control law.

Section 4 is devoted to navigation. The basic motion sensor package that is used to estimate the position and attitude of the vehicle is presented. The design of its navigation system based on single and multi-rate Kalman filtering techniques is briefly described.

*This work was supported in part by the Commission of the European Communities under contracts MAST-CT90-0059 and MAS2-CT92-0021 of the the Marine Science and Technology Programmes (MAST-I and II) and in part by JNICT under contract PMCT/C/TIT/702/90.

0-7803-1808-0/94 $4.00 © 1994 IEEE

Finally, Section 5 combines guidance with navigation and control. For a given reference trajectory, the dynamic performance of the vehicle is examined when the classical guidance algorithm of line-of-sight is used. The integrated simulation package that supports this study has been developed and implemented on a SUN-SPARC station. It is written in C language, and runs under the MATRIXx software package for computer aided control systems design.

2 Vehicle Modelling

This section describes the dynamical model of the AUV MARIUS that is used for simulation and control systems design. The vehicle is depicted in figure 1. See [6, 7] for a complete description of the vehicle's design and construction. The general structure of the model is standard,

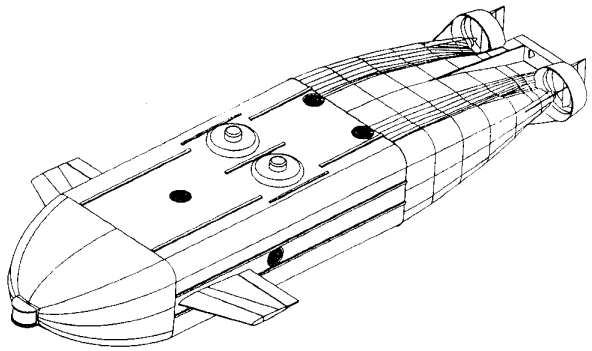

Figure 1: The vehicle MARIUS

and was simply derived from first physics principles, as explained in [1]. System identification, however, was far more complex and required the combination of theoretical and experimental methods that included tank tests with the full scale prototype of the vehicle. The tests are reported in [7, 22]. The estimated model can be found in [11], which contains a description of the methodologies used for modelling and identification.

2.1 Equations of Motion

The equations of motion for underwater vehicles can be obtained from Newton-Euler laws following the classical approach described by Abkowitz [1]. A simple and elegant derivation based on a general set-up adopted in robotics [4]can be found in [27]. Using this approach, the equations are easily developed using a global coordinate frame $\{U\}$ and a body-fixed coordinate frame $\{B\}$ that moves with the AUV. This requires the following notation, adapted from [4] and [8]:

${}^{U}\mathbf{p}_{B_{org}} := (x, y, z)^T$ - position of the origin of $\{B\}$ measured in $\{U\}$,

${}^{B}\mathbf{v}_{B_{org}} := (u, v, w)^T$ - velocity of the origin of $\{B\}$ relative to $\{U\}$, expressed in $\{B\}$ (i.e., body-fixed linear velocity),

${}^{B}\boldsymbol{\omega}_{B} := (p, q, r)^T$ - angular velocity of $\{B\}$ relative to $\{U\}$, expressed in $\{B\}$ (i.e., body-fixed angular velocity).

The symbol ${}^{U}_{B}R(\boldsymbol{\lambda})$ denotes the rotation matrix from $\{B\}$ to $\{U\}$, parameterized by the vector $\boldsymbol{\lambda}:=(\phi, \theta, \psi)^T$ of roll, pitch and yaw angles. Furthermore, $\dot{\mathbf{q}} = (u, v, w, p, q, r)^T$ and $\boldsymbol{\delta} := (\delta_{a,c}, \delta_{a,d}, \delta_e, \delta_r)^T$ denote the body-fixed linear and angular velocity vector and the vector whose entries correspond to deflections of the ailerons (common and differential), elevator, and rudder, respectively. The symbol n denotes the propeller rotational rate. With this notation, the dynamics and kinematics of the AUV can be written in compact form as

Dynamics:

$$M_{RB}\ddot{\mathbf{q}} + C_{RB}(\dot{\mathbf{q}})\dot{\mathbf{q}} = \boldsymbol{\tau}(\ddot{\mathbf{q}}, \dot{\mathbf{q}}, \boldsymbol{\lambda}, \boldsymbol{\delta}, n), \tag{1}$$

$$\mathbf{q} = ({}^{B}\mathbf{v}^T_{B_{org}}, {}^{B}\boldsymbol{\omega}^T_{B})^T. \tag{2}$$

Kinematics:

$$\frac{d}{dt}({}^{U}\mathbf{p}_{B_{org}}) = {}^{U}_{B}R(\boldsymbol{\lambda}){}^{B}\mathbf{v}_{B_{org}}, \tag{3}$$

$$\frac{d}{dt}\boldsymbol{\lambda} = Q(\boldsymbol{\lambda}){}^{B}\boldsymbol{\omega}_{B}, \tag{4}$$

where $\boldsymbol{\tau}$ denotes the vector of external forces and moments and $Q(\boldsymbol{\lambda})$ is the matrix that relates body-fixed angular velocity with roll, pitch and yaw rates. The symbols M_{RB} and C_{RB} denote the rigid body inertia matrix and the matrix of Coriolis and centrifugal terms, respectively.

The vector $\boldsymbol{\tau}$ can further be decomposed as

$$\begin{aligned}\boldsymbol{\tau}(\ddot{\mathbf{q}}, \dot{\mathbf{q}}, \boldsymbol{\lambda}, \boldsymbol{\delta}, n) &= \boldsymbol{\tau}_{rest}(\boldsymbol{\lambda}) \\ &+\boldsymbol{\tau}_{add}(\ddot{\mathbf{q}}, \dot{\mathbf{q}}) + \boldsymbol{\tau}_{lift}(\dot{\mathbf{q}}, \boldsymbol{\delta}) \\ &+\boldsymbol{\tau}_{visc}(\dot{\mathbf{q}}, \boldsymbol{\delta}) + \boldsymbol{\tau}_{prop}(n),\end{aligned} \tag{5}$$

where $\boldsymbol{\tau}_{rest}$ denotes the the forces and moments caused by gravity and buoyancy and $\boldsymbol{\tau}_{add}$ (added mass term) accounts for the dynamic forces and moments that would act on the vehicle assuming it were completely submerged in an inviscid fluid with no circulation. The term $\boldsymbol{\tau}_{lift}$ captures the effects of the lifting forces generated by the deflecting surfaces, $\boldsymbol{\tau}_{visc}$ consists of the forces and moments caused by skin friction and $\boldsymbol{\tau}_{prop}$ represents the forces and moments generated by the main propellers. The following notation will be used in the text: $\mathbf{V} = (u^2 + v^2 + w^2)^{1/2}$ denotes the absolute value of the velocity vector, $\alpha = arcsin(w/(u^2 + w^2)^{1/2})$ is the angle of attack and $\beta = arcsin(v/(u^2 + v^2 + w^2)^{1/2})$ is the angle of side-slip.

2.2 System Identification

To be of practical use, the model described by equations (1)-(4) must be tuned for the vehicle in study. Clearly, the main difficulty lies in computing the term τ that arises in the equation of dynamics. This was achieved by using both theoretical and experimental methods.

The restoring term was easily computed from geometrical considerations, and the added mass term was computed by assuming ellipsoidal and elliptical cylinder approximations for the body and ailerons, respectively [18, 23]). Approximations for the lift term were obtained using thin airfoil theory [14].

The viscous damping and propulsion terms were determined from the following series of tests carried out at the Danish Maritime Institute (DMI) in Lyngby, Denmark:

- Open water tests of the propeller/nozzle system to determine its characteristics in undisturbed (open) water,
- Resistance tests to measure the resistance of the vehicle without the propulsion system in place,
- Self-propulsion tests to assess the performance of the propulsion system in the wake of the hull,
- Planar Motion Mechanism tests in the horizontal and vertical planes to measure the most relevant hydrodynamic derivatives of the vehicle.

The methodology used for testing is reported in [7] and follows the main guidelines exposed in [1, 12]. Complete test results can be found in [22, 26]. See also [10, 11] for a description of the derived model used for simulation.

For control design purposes, the general model was divided into two sub-models for the horizontal and vertical planes. This procedure is standard [13],and fully justified for the case when the vehicle executes maneuvers that require only light interaction between steering in the horizontal plane and diving in the vertical plane. The sub-models do not include the kinematics equation (3), which is only relevant to the guidance system. In order to simplify the design phase, the vehicle was assumed to be commanded directly in thrust. Based on theoretical and experimental results available from tank tests, the simplified vertical model can then be written as

Surge Motion Equation:

$$\begin{aligned} m\dot{u} + mqw &= \frac{\rho}{2}L^2 X_{u^2} u^2 + \frac{\rho}{2}L^2 u^2 \left[X_{\delta^2_{a,c}}\delta^2_{a,c} + X_{\delta^2_e}\delta^2_e\right] \\ &\quad + \frac{\rho}{2}L^2 X_{w^2} w^2 + \frac{\rho}{2}L^3 X_{\dot{u}}\dot{u} + T, \end{aligned}$$

Heave Motion Equation:

$$\begin{aligned} m\dot{w} - mqu &= \frac{\rho}{2}L^2 u^2 \left[Z_{\delta_{a,c}}\delta_{a,c} + Z_{\delta_e}\delta_e\right] + \frac{\rho}{2}L^2 u Z_w w \\ &\quad + \frac{\rho}{2}L^3 Z_{\dot{w}}\dot{w} + \frac{\rho}{2}L^4 Z_{\dot{q}}\dot{q}, \end{aligned}$$

Pitch Motion Equation:

$$\begin{aligned} I_y\dot{q} &= z_{CB}Bsin(\theta) + \frac{\rho}{2}L^3 u^2 \left[M_{\delta_{a,c}}\delta_{a,c} + M_{\delta_e}\delta_e\right] \\ &\quad + \frac{\rho}{2}L^3 u M_w w + \frac{\rho}{2}L^4 u M_q q + \frac{\rho}{2}L^4 M_{\dot{w}}\dot{w} \\ &\quad + \frac{\rho}{2}L^5 M_{\dot{q}}\dot{q}, \\ \dot{\theta} &= q, \end{aligned}$$

where X_{u^2}, ..., $M_{\dot{q}}$ are nondimensional hydrodynamic coefficients [1], ρ is the density of the water, and $L = 4.2\,m$ and m are the length and mass of the vehicle, respectively. The symbol B denotes the buoyancy of the vehicle, $\mathbf{r}_{CB} = (0, 0, z_{CB})^T$ and $\mathbf{r}_{CG} = (0, 0, 0)^T$ are the positions of the center of gravity and buoyancy respectively, measured in the body-frame B, and I_y is the moment of inertia about the yy axis. The symbol T represents the thrust generated by the propulsion system. The numerical values of the parameters can be found in Table 1. It is important

m	=	$2234.5Kg$,	B	=	$21898N$,
ρ	=	$1025Kg/m^3$,	z_{CB}	=	$-4.1e^{-2}m$,
I_y	=	$1700Kgm^2$,	g	=	$9.8m/s^2$
X_{u^2}	=	$-5.34e^{-3}$,	$M_{\delta_{a,c}}$	=	$5.88e^{-3}$,
$X_{\delta^2_{a,c}}$	=	$-7.75e^{-3}$,	M_{δ_e}	=	$3.93e^{-3}$,
$X_{\delta^2_e}$	=	$-9.81e^{-3}$,	M_w	=	$7.72e^{-2}$,
X_{w^2}	=	$-2.42e^{-1}$,	M_q	=	$-3.76e^{-2}$,
$X_{\dot{u}}$	=	$-3.62e^{-3}$,	$M_{\dot{w}}$	=	$-6.08e^{-3}$,
$Z_{\delta_{a,c}}$	=	$-3.22e^{-2}$,	$M_{\dot{q}}$	=	$-8.74e^{-3}$,
Z_{δ_e}	=	$-9.05e^{-3}$,	$Z_{\dot{w}}$	=	$-1.21e^{-1}$,
Z_w	=	$-2.58e^{-1}$,	$Z_{\dot{q}}$	=	$-6.08e^{-3}$.

Table 1: Vertical model parameters

to stress that the experimental test conditions [7] impose strict restrictions on the region of validity of the vertical sub-model. In fact, the model applies only to small vertical motions about the equilibrium, or trimming conditions determined by $v_0 = w_0 = p_0 = q_0 = r_0 = \phi_0 = \theta_0 = 0$, and $\delta_{a,c_0} = \delta_{a,d_0} = \delta_e = \delta_r = 0$. With this restriction, the vertical model can be formally written as

$$\frac{d}{dt}\mathbf{x}_v = \mathbf{f}_v(\mathbf{x}_v, \mathbf{u}_v), \tag{6}$$

where $\mathbf{x}_v = (u, w, q, \theta)^T \in \mathcal{R}^4$ is the state vector, $\mathbf{u}_v = (\delta_{a,c}, \delta_e, T)^T \in \mathcal{R}^3$ is the input vector and $\mathbf{f}_v : \mathcal{R}^4 \times \mathcal{R}^3 \rightarrow \mathcal{R}^4$ is a nonlinear function that is easily obtained from the surge, heave and pitch equations of motion.

Identical procedure can be applied to the horizontal plane to obtain the compact description $\frac{d}{dt}\mathbf{x}_h = \mathbf{f}_h(\mathbf{x}_h, \mathbf{u}_h)$, where $\mathbf{x}_h = (v, p, r, \phi, \psi)^T$ is the state vector and $\mathbf{u}_h = (\delta_{a,d}, \delta_r)^T$ is the input vector. The horizontal model is not detailed here.

The expected performance of the vehicle in terms of stability, maneuverability, and mission duration and range can been determined from the general model derived in [11]. Mission duration and range were determined in [7]. Stability and maneuverability were thoroughly studied in [11], from which figure 2 was taken as an illustrative example. The figure depicts the trimming conditions δ_{e_o} and δ_{a,c_0} for the elevator and (common) aileron deflection angles, respectively, as functions of pitch angle θ. The parameter u_o sets the trimming for forward speed. The curves were determined with the angle of attack α set to zero. At a forward speed of $2.0m/s$, the vehicle can sustain

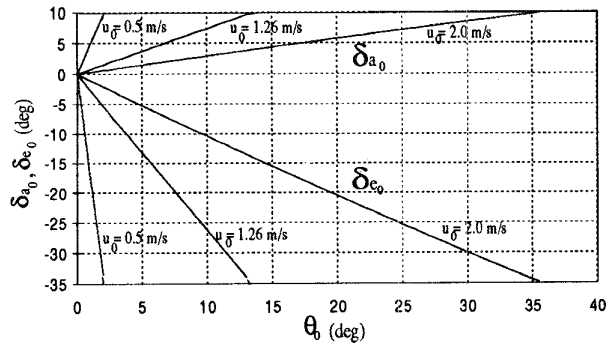

Figure 2: Trimming conditions in pitch angle

a pitch angle of 30 *deg* with the deflection of the ailerons and elevator set to 8 *deg* and -30 *deg*, respectively.

3 Control System Design

This section focuses on the design of a control system for the AUV MARIUS. The methodology adopted is gain-scheduled control, whereby the design of a controller to achieve stabilization and adequate performance of a given nonlinear plant (system to be controlled) involves the following steps:

i) Linearizing the plant about a finite number of representative operating points,

ii) Designing linear controllers for the plant linearizations at each operating point,

iii) Interpolating the parameters of the linear controllers of Step ii) to achieve adequate performance of the linearized closed-loop systems at all points where the plant is expected to operate. The interpolation is performed according to an external scheduling vector (e.g., dynamic pressure and angle of attack), and the resulting family of linear controllers is referred to as *gain scheduled controller*,

iv) Implementing the gain scheduled controller on the original nonlinear plant.

The methodology selected for linear control system design is $\mathcal{H}_\infty$ [5]. This method rests on a firm theoretical basis, and leads naturally to an interpretation of control design specifications in the frequency domain. Furthermore, it provides clear guidelines for the design of controllers so as to achieve robust performance in the presence of plant uncertainty. The implementation of the gain-scheduled controller was done using a new methodology, henceforth referred to as the $\mathcal{D}$-methodology. See [16] for the theorical framework and Section 3.5 for a short description of the practical implementation aspects. In this section, due to space limitations, we only illustrate the design of a controller for the vertical plane about a single operating condition.

3.1 Linearization. Open-Loop System Analysis

The following notation is required. Given a nonlinear dynamical system $\mathcal{S}$ described by $\frac{d}{dt}\mathbf{x} = \mathbf{f}(\mathbf{x},\mathbf{u})$; $\mathbf{y} = x$, where $\mathbf{f} : \mathcal{R}^n \times \mathcal{R}^m \rightarrow \mathcal{R}^n$ is of class C^1, the vector $(\mathbf{x}_0^T, \mathbf{u}_0^T)^T \in \mathcal{R}^n \times \mathcal{R}^m$ is called an equilibrium point of $\mathcal{S}$ if $\mathbf{f}(\mathbf{x}_0, \mathbf{u}_0) = 0$. The linearization of $\mathcal{S}$ about the equilibrium point $(\mathbf{x}_0, \mathbf{u}_0)$ is the linear system with realization $\{A, B, C\}$, where $A = A(\mathbf{x}_0, \mathbf{u}_0) = \frac{\partial}{\partial \mathbf{x}}\mathbf{f}(\mathbf{x}_0, \mathbf{u}_0)$, $B = B(\mathbf{x}_0, \mathbf{u}_0) = \frac{\partial}{\partial \mathbf{x}}\mathbf{f}(\mathbf{x}_0, \mathbf{u}_0)$ and $C = I$.

The model for the vertical plane was rewritten in terms of the angle of attack α and total velocity $\mathbf{V}$, and linearized about the equilibrium point determined by $\mathbf{x}_0 = (\mathbf{V}_0, \alpha_0, q_0, \theta_0)^T = (1.26\ m/s, 0, 0, 0)^T$ and $\mathbf{u}_0 = (\delta_{a,c_0}, \delta_{e_0}, T_0)^T = (0, 0, 77.2N)^T$. Close examination of the structure of the linearized model revealed the following.

The state matrix for the linearized plant model exhibits one stable, second order lightly damped mode with a natural frequency of 0.19 *rad/s* that is associated with θ. This mode couples itself to angle of attack α, and to the angular rate q. There is also a real pole at $s = -1.4$ *rad/s* that couples the same state variables. Notice that θ does not exhibit a pure integration effect, due to the existence of a restoring torque caused by buoyancy and gravity. Forward speed $\mathbf{V}$ is decoupled from the other state variables and presents a real pole at $s = -0.05$ *rad/s*. As for the input matrix, the elevator deflection δ_e and the (common mode) aileron deflection $\delta_{a,c}$ affect the evolution of θ, α and q. Thrust T affects forward speed $\mathbf{V}$, only.

3.2 Design Requirements

The linear controller was required to satisfy the following design requirements:

1. **Zero Steady State Error.** Achieve zero steady state values for all error variables in response to command inputs in pitch (θ_{cmd}), angle of attack (α_{cmd}) and forward velocity ($\mathbf{V}_{cmd}$).

2. **Bandwidth Requirements.** The input-output command response bandwidth for all command channels should be on the order of 0.1 *rad/s*; the control loop bandwidth for all actuators should not exceed 0.5 *rad/s* (these figures were selected to ensure that the actuators were not be driven beyond their normal bandwidth).

3. **Closed Loop Damping and Stability Margins.** The closed loop eigenvalues should have a damping ratio of a least 0.6. Classical gain and phase margins of 6 *db* and 45 *deg* should be satisfied in all control loops (one loop at a time analysis).

3.3 Linear Control System Design: The $\mathcal{H}_\infty$ Synthesis Approach

The controller for the linearized vertical model was designed using $\mathcal{H}_\infty$ synthesis theory. See [5] for an elegant solution to this problem using a state-space framework

and [17] for a case study. In what follows, we adopt the

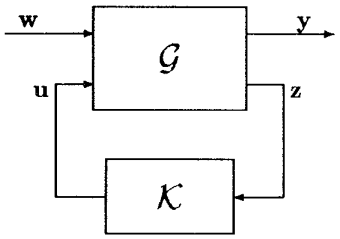

Figure 3: Feedback interconnection.

general set-up and nomenclature in [5]. This leads to the standard feedback system of figure 3, where $\mathbf{w}$ is the input vector of exogenous signals, $\mathbf{z}$ is the output vector of errors to be reduced, $\mathbf{y}$ is the vector of measurements that are available for feedback and $\mathbf{u}$ is the vector of actuator signals. The generalised plant $\mathcal{G}$ consists of the plant to be controlled, together with appended weights that shape the exogenous and internal signals, see Section 3.4. Suppose that the feedback system is well-posed, and let $\mathcal{T}_{\mathbf{zw}}$ denote the closed loop transfer matrix from $\mathbf{w}$ to $\mathbf{z}$. The $\mathcal{H}_\infty$ synthesis problem consists of finding, among all controllers that yield a stable closed loop system, a controller K that minimises the infinity norm $\|\mathcal{T}_{\mathbf{zw}}\|_\infty$ of the operator $\mathcal{T}_{\mathbf{zw}}$. We remind the reader that $\|\mathcal{T}_{\mathbf{zw}}\|_\infty$ equals $\sup\{\sigma_{\max}(\mathcal{T}_{\mathbf{zw}}(j\omega)) : \omega \in \Re\}$, where $\sigma_{max}(.)$ denotes the maximum singular value of a matrix. The norm $\|\mathcal{T}_{\mathbf{zw}}\|_\infty$ may be interpreted as the maximum energy gain of the closed loop operator $\mathcal{T}_{\mathbf{zw}}$. Throughout this paper we assume that all states are available for measurement, that is, $\mathbf{y}$ equals the internal state of the extended plant $\mathcal{G}$.

Suppose that a state-space realization for $\mathcal{G}$ can be written as

$$\begin{aligned} \dot{\mathbf{x}} &= A\mathbf{x} + B_1\mathbf{w} + B_2\mathbf{u} \\ \mathbf{z} &= C_1\mathbf{x} + D_{12}\mathbf{u} \\ \mathbf{y} &= \mathbf{x}, \end{aligned}$$

and assume that (A, B_2) is stabilizable, D_{12} has linearly independent columns, and that the system with input $\mathbf{u}$ and output $\mathbf{z}$ has no zeros on the imaginary axis. The key mathematical result on $\mathcal{H}_\infty$ synthesis that we use in the present work is stated below.

Theorem 3.1 *Suppose $\gamma > 0$ is a given positive number, and let*

$$H(\gamma) = \begin{bmatrix} H_{11} & H_{12} \\ H_{21} & H_{22} \end{bmatrix}$$

denote the Hamiltonian matrix with entries

$$\begin{aligned} H_{11} &= A - B_2(D_{12}^T D_{12})^{-1} D_{12}^T C_1 \\ H_{12} &= \gamma^{-2} B_1 B_1^T - B_2(D_{12}^T D_{12})^{-1} B_2^T \\ H_{21} &= -C_1^T(I - D_{12}(D_{12}^T D_{12})^{-1} D_{12}^T) C_1 \\ H_{22} &= -A^T + C_1^T D_{12}(D_{12}^T D_{12})^{-1} B_2^T. \end{aligned}$$

Then, there exists a stabilising controller K such that $\|\mathcal{T}_{\mathbf{zw}}\| < \gamma$ if and only if

i) $H(\gamma)$ has no eigenvalues on the imaginary axis and there exists a basis for the spectral subspace $\chi_-(H(\gamma))$ of $H(\gamma)$ of the form $[X_1', X_2']'$, where X_1 and X_2 are square matrices of appropriate dimensions and X_1 is invertible

ii) $X(\gamma) := X_2 X_1^{-1}$ is positive semi definite.

In this case, one such static controller is $\mathcal{K} = F$, where

$$F = -(D_{12}^T D_{12})^{-1}[D_{12}^T C_1 + B_2^T X(\gamma)].$$

Existence and computation of $X(\gamma)$ is a standard matrix algebra problem that can be solved using a standard technique for solving Riccati equations based on the real Schur decomposition [19].

In practice, this theorem is used in the following way. First, a stabilizing state feedback gain matrix K is computed using the aforementioned formulas with $\gamma = \infty$ (this step yields the optimal gain for the $\mathcal{H}_2$ problem). The infinity norm of the resulting closed-loop transfer matrix $\mathcal{T}_{\mathbf{zw}}$ is then computed using the algorithm in [3]. This, in turn, gives an upper bound γ_u on the achievable performance. The theorem is then used to perform a binary search in the interval $[0,\ \gamma_u]$ for the optimal value of γ. Once the binary search has determined a sufficiently small interval in which the optimal value of γ must lie, the search is stopped and a (suboptimal) state feedback gain matrix $\mathcal{K}$ is computed using the right endpoint of this interval for γ in the formulas above.

3.4 Synthesis Model and Controller Design

The first step in the controller design procedure is the development of a synthesis model which can serve as an interface between the designer and the $\mathcal{H}_\infty$ controller synthesis algorithm. Consider the feedback system shown in Figure 4, where $\mathcal{P}$ is the linearized model of the AUV in the vertical plane and $\mathcal{K}$ is the controller to be designed. The block $\mathcal{G}$ within the dashed line is the synthesis model, which is derived from the linear model of the plant by appending the depicted weights. In practice, the weights serve as tuning "knobs" which the designer can adjust to meet the desired performance specifications.

The signal $\mathbf{w}_1$ represents the vector of input commands which must be tracked. It consists of velocity, angle of attack and pitch commands, denoted $\mathbf{V}_{cmd}$, α_{cmd} and θ_{cmd}, respectively. The signal $\mathbf{w}_2$ represents the noise inputs to each of the sensors, and disturbance inputs to the states of the plant. The signal $\mathbf{u}$ represents the control inputs to the system. It consists of the actuator signals for common aileron deflection $\delta_{a,c}$, elevator deflection δ_e and thruster command T. The signal $\mathbf{x}_1$ represents the components of the state vector that must track the input commands and consists of $\mathbf{V}$, α and θ. The vector

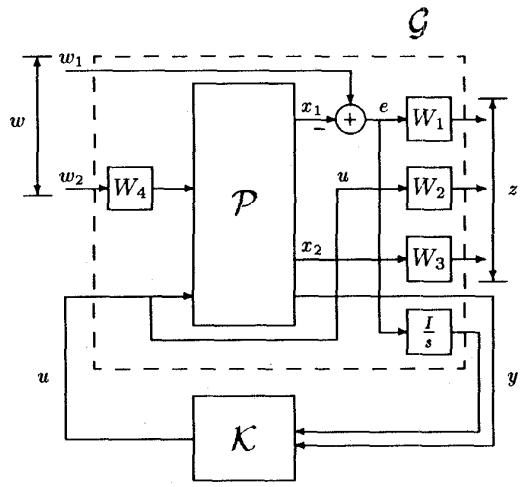

Figure 4: Synthesis model.

$\mathbf{e} = \mathbf{w}_1 - \mathbf{x}_1 = (\mathbf{V}_e, \theta_e, \alpha_e)^T$ contains the respective tracking errors. The signal $\mathbf{x}_2$ contains the remaining state variable - pitch rate q - that must be weighted.

The outputs of W_1, W_2, and W_3 constitute the vector $\mathbf{z}$. Since zero steady-state errors in tracking the step command for all variables in $\mathbf{x}_1$ was required, the weighting function W_1 was chosen as

$$W_1 = \begin{pmatrix} \frac{2}{s} & 0 & 0 \\ 0 & \frac{1}{s} & 0 \\ 0 & 0 & \frac{1}{s} \end{pmatrix},$$

where the integrator gains were adjusted to get the desired command response bandwidths. The weights W_2 and W_3 do not need include any dynamics. The elements of $W_2 = diag(1,\ 1,\ 0.1)$ were adjusted to meet the additional desired specifications. The weight W_3 was set equal to 1. The signal $\mathbf{y}$ includes all the states of the plant $\mathcal{P}$, together with the appended states that correspond to the integrators, that is, $\mathbf{y}$=($\mathbf{V}$, α, q, θ, $\frac{V_e}{s}$, $\frac{\alpha_e}{s}$, $\frac{\theta_e}{s}$).

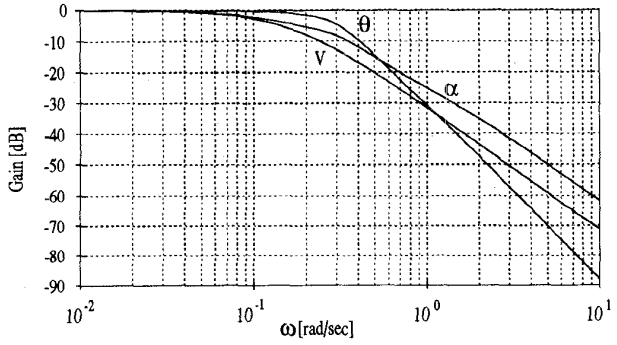

Figure 5: Closed loop frequency responses.

The performance of the resulting controller is illustrated in figures 5 and 6. Figure 5 depicts the closed loop frequency responses from the command signals θ_{cmd}, α_{cmd}, and V_{cmd} to the corresponding outputs. Figure 6 shows the closed-loop step responses. Notice that the overshoot associated with the pitch angle θ meets the design specifications. Furthermore, the angle of attack and speed responses do not overshoot.

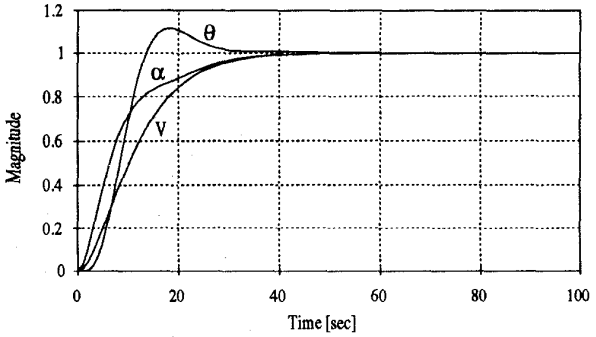

Figure 6: Closed loop step responses.

3.5 Non-linear Controller Implementation

A set of controllers was determined for three values of forward speed, and their parameters interpolated according to the scheduling variable $\mathbf{V}$, see [11]. The implementation of the resulting non-linear gain scheduled controller was done using the D-methodology described in [16]. This approach guarantees the following fundamental *linearization property*: at each equilibrium point, the linearization of the nonlinear feedback control system preserves the internal as well as the input-output properties of the corresponding linear closed loop designs. This property is often not satisfied in gain scheduled controllers proposed in the literature, see [16] and the references therein. In practice, violation of that property may lead to degradation in performance, or even instability, of the closed -loop system.

The method is based on the key observation that linear controllers are designed to operate on the perturbations of the plant's inputs and outputs about the equilibrium points. Proper blending of the different controllers requires that they have access to such perturbations, locally. This is achieved by differentiating some of the measured outputs before they are fedback to the gain scheduled controller. In order to preserve the input- output behaviour of the feedback system, integral action is provided at the input to the plant. Despite the use of differentiators, this scheme does not introduce additional noise amplification at the relevant inputs and outputs of the feedback system, since all closed loop transfer functions are preserved. Furthermore, the resulting nonlinear gain scheduled controller is easy to obtain, and its structure is similar to that of the original linear controllers. The existence of integrators directly at the input of the plant makes the implementation of anti-windup schemes straightforward [9].

The controller implementation is depicted in figure 7, where $F(V)$ denotes the block for interpolating the state

feedback gains obtained from the linear design methodology exposed in Section 3.3. It is important to stress that the $\mathcal{D}$-method presented above requires differentiating some of the plant's measured outputs. Except for the case where some of the derivatives are available from dedicated sensors, this cannot be done in practice. In this case, the differentiation operator may simply replaced by a causal system with transfer function $\frac{s}{\tau s+1}$, as shown in the figure, or by a simple finite difference operator for discrete-time implementation, see [16].

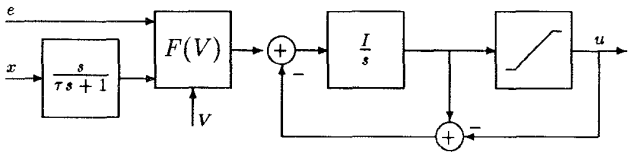

Figure 7: Controller implementation.

4 Navigation System Design

This section describes the basic framework used in the design of the navigation system for the AUV MARIUS. The objective is to obtain accurate estimates of the position and attitude of the vehicle, based on measurements available from a motion sensor package installed on-board. The estimates are input to the controller derived in section 3, and to the guidance system that wil be described in section 5.

From a theoretical point of view, the navigation system design problem can be reduced to that of estimating the state of a nonlinear plant from which observations corrupted with noise are available. Plant nonlinearities are clearly displayed in the dynamic equations of motion derived in section 2, and noise is inherent to sensor measurements. This estimation problem has been thoroughly studied in the literature, and under certain conditions solutions can be found within the framework of Extended Kalman Filtering theory [28]. However, the computational burden associated with the implementation of the filters proposed, and their possible lack of robustness against mismatches between the nonlinear design model and the dynamics of the vehicle, preclude their use in real time applications.

In this paper we adopt an alternative, conceptually simple framework for filtering, that is rooted in the kinematic relationships expressed by equations (3) and (4). This approach borrows from the theory of *complementary filtering*. See [20]for a lucid presentation of the subject, and [8, 20] for interesting applications to aircraft and underwater vehicle navigation systems. That approach leads naturally to the design of linear, time-invariant Kalman filters, whereby the covariance of the process and observation noises are viewed as tuning knobs to shape the frequency responses from measured to estimated variables. This methodology bears great affinity with the general procedure for control system design explained in section 3. In the case of pitch estimation, for example, it leads to a systematic procedure to weight the relative contribution of pitch and pitch rate measurements based on the quality of sensor data (see section 4.1).

Due to space limitations, the complete navigation system design procedure is not detailed in this paper. Sections 4.1and 4.2contain only a brief description of the sensors used in the vehicle, as well as the navigation design requirements and the basic filter structures adopted. Complete details are available in [10].

4.1 Attitude Estimation

The motion sensor package of MARIUS includes two *pendulums* that provide indirect measurements ϕ_p [1] and θ_p of roll and pitch angles, respectively, one *gyrocompass* that provides measurements (ψ_c) of yaw angle, and three *rate gyroscopes* whose outputs p_r, q_r, r_r correspond to the angular body rates p, q, r.

The design of a filter to provide corrected estimates of roll, pitch and yaw angles and of angular body rates based on the information available from the sensors, follows the basic methodology exposed in [20]. In its simplest form, that technique requires that the evolution of $\boldsymbol{\lambda}=(\phi,\theta,\psi)^T$ be interpreted as the output of a system of three double integrators driven by gaussian, white noise (state model). The state of the system consists of $\boldsymbol{\lambda}$ and $\frac{d}{dt}(\boldsymbol{\lambda})$, thus reflecting the obvious fact that the derivative of position is velocity, and the derivative of velocity is acceleration (which is not known). Measurements of $\boldsymbol{\lambda}$ are obtained by simple manipulation of the information available from ϕ_p, θ_p and ψ_c. Measurements of $\frac{d}{dt}\boldsymbol{\lambda}$ are obtained from rate gyro data using the kinematics equation (4). It is also assumed that the measurements are corrupted by gaussian, white noise. By discretizing the state model, one is led to the formal description [2]

$$\begin{aligned}\mathbf{x}_{k+1} &= F\mathbf{x}_k + G\mathbf{w}_k \\ \mathbf{z}_k &= H\mathbf{x}_k + \mathbf{v}_k,\end{aligned}$$

where $\mathbf{x}$ is the state vector, $\mathbf{z}$ is the measurement vector, and $\mathbf{w}$ and $\mathbf{v}$ are zero mean, gaussian, uncorrelated stochastic processes with covariance matrices

$$E[\mathbf{w}_k\mathbf{w}_j^T] = Q\delta_{kj}, E[\mathbf{v}_k\mathbf{v}_j^T] = R\delta_{kj},$$

where δ_{kj} denoted the Kronecker operator. Under some technical assumptions, the stationary filter that minimizes the mean-square error estimation of $\mathbf{x}$ based on the observations $\mathbf{z}$, is asymptotically stable, and is given by the Kalman filter structure [28]

$$\hat{\mathbf{x}}_{k+1} = F\hat{\mathbf{x}}_k + K(\mathbf{z} - H\hat{\mathbf{x}}_k)$$

where $\hat{\mathbf{x}}$ denotes the best estimate of $\mathbf{x}$, and

$$K = PH^T(HPH^T + R)^{-1}$$

[1] Subscripts indicate variables that are measured by sensors.

[2] The subscript k is an abbreviation of kh, where h is the sampling period.

is obtained from the positive semidefinite solution P to the algebraic Riccati equation

$$P = FPF^T - FPH^T(HPH^T + R)^{-1}HPF^T + GQG^T.$$

Again, it must be stressed that the covariance matrices Q and R serve as weights to shape the transfer functions between $\mathbf{z}$ and the estimate $\hat{\mathbf{x}}$ of $\mathbf{x}$.

For the sake of clarity, the synthesis of a Kalman filter to estimate pitch angle based on corrupted measures of pitch and pitch rate is presented below. Without loss of generality, we assume that roll and yaw are zero. The following design requirements are specified:

1. **Zero Steady State Estimate Error.** Pitch and pitch rate estimation errors should be driven assymptotically to zero when the vehicle is following a trajectory with zero angular acceleration (in particular, the filter should reject constant rate gyro bias terms).

2. **Bandwidth Requirements.** The filter bandwidths corresponding to the transfer functions from pitch and pitch rate measurements to to the corresponding estimates should be on the order of $15 rad/sec$ $(3Hz)$, that is, approximately one decade bigger than that of the corresponding control loops (see section 3).

Using the formalism exposed above and adopting a sampling frequency of $100\,Hz$, the choice of covariance matrices

$$Q = \begin{bmatrix} 100.0 & 0.0 \\ 10.0 & 1.0 \end{bmatrix} \quad \text{and} \quad R = \begin{bmatrix} 0.1 & 0.0 \\ 10.0 & 1.0 \end{bmatrix}$$

leads to a filter with the Bode diagram of figure 8. Notice how the estimator relies on the information provided by the pendulum at low frequency. At high frequency,the estimator relies essentially on the integral of measured pitch rate.

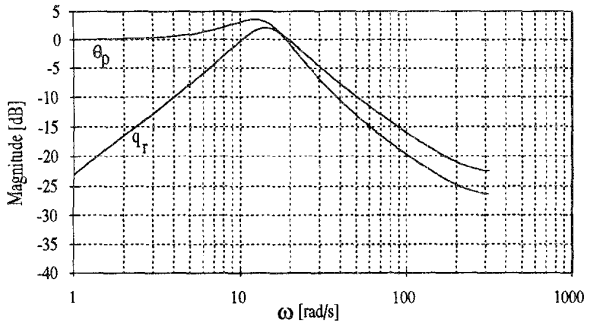

Figure 8: Bode diagrams - transfer functions from q_r and θ_p to estimate $\hat{\theta}$.

4.2 Linear Position and Velocity Estimation

The following sensor units are used to provide measurements of the linear position and velocity of the vehicle: a *long baseline positioning system* (LBL) that computes the roundtrip travel times of acoustic pulses that are emitted by the vehicle and returned by an array of transponders (a triangulation algorithm is used to provide measurements of ${}^{U}\mathbf{p}_{B_{org}} := (x, y, z)^T$), a *depth cell* that provides direct measurements of depth coordinate z, and a Doppler sonar that measures the body fixed velocity vector ${}^{B}\mathbf{v}_{B_{org}} := (u, v, w)^T$. A simple *paddle wheel* sensor is used as a back-up instrument to provide measurements of u_w, where the subscript denotes that the velocity is computed with respect to the water.

An integrated filter to provide corrected estimates of position and velocity of the vehicle with respect to the seabed can now be designed following an approach similar to that described in section 4.1. Notice, however, that due to the characteristics of the acoustic channel, the measurements from the LBL system are available at a rate that is much smaller than that of the remaining sensors. This problem can be tackled using multi-rate Kalman filter theory exposed in [21, 29]. See [10] for the design of a multi-rate filter for the vehicle, where the sampling rate of the LBL system and that of the other sensors are $1\,Hz$ and $10\,Hz$, respectively.

5 Guidance. Integrated Simulation with Navigation and Control.

The purpose of the guidance system is to generate the references that are applied to the AUV's control system in order to achieve accurate tracking of trajectories specified in a universal reference frame $\{U\}$. Conceptually, the design of the guidance system is rather simple as it relies solely on the kinematics equation (3) of Section 2. The basic strategy involved is easily explained by restricting the motion of the vehicle to the horizontal plane, and by assuming that the vehicle progresses at constant forward speed $\mathbf{V}$ with a small sideslip angle β. In this case, the role of the guidance system is reduced to computing the reference command ψ_{cmd} for yaw angle ψ so that the x-body axis of the vehicle will point to an imaginary point located on the reference trajectory, at a certain visibility distance d ahead of the vehicle. The guidance law used in this study is a slight modification of that reported in [13]. See [11]for details, and for a complete study on the choice of the visibility distance d.

The combined performance of the guidance, navigation and control systems was evaluated in simulation with the nonlinear model of the vehicle. The simulation included also physically based models of the sensor units described in section 4 In order to simplify the interpretation of the simulation results, the velocity command $\mathbf{V}_c$ was held constant at $1.26 m/s$. The references to roll and angle of attack were set to zero.

The reference for linear position is an U - shaped trajectory that descends smoothly along the depth coordinate z. Its projection on the horizontal plane consists of two straight lines joined by a semi-circumference

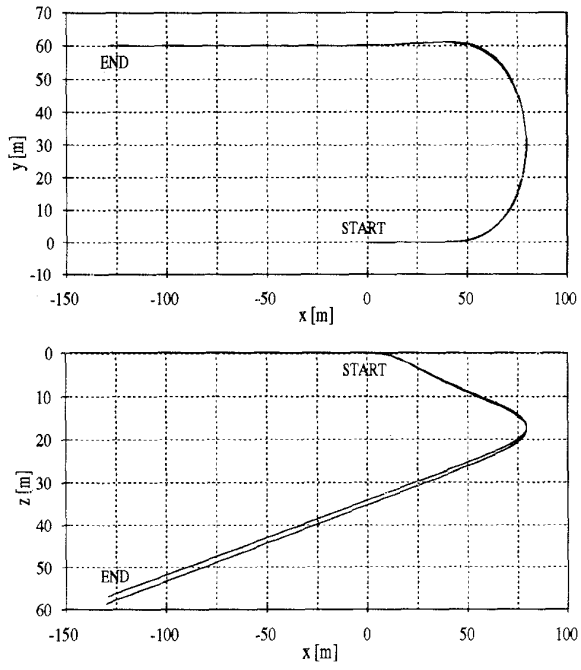

Figure 9: Reference and observed trajectory - horizontal and vertical planes.

with a radius of 30 m. The projection on the vertical plane consists roughly of two straight lines with a slope of -10 deg. The desired and observed trajectories are depicted in figure 9. The evolution of the control inputs and the activity of some relevant state variables are condensed in figures 10, 11 and 12. In this simulation, the LBL system uses four transponders located in positions $\{-40, 0, 160\}, \{90, 0, 150\}, \{-40, 60, 170\}$ and $\{90, 60, 135\}$.

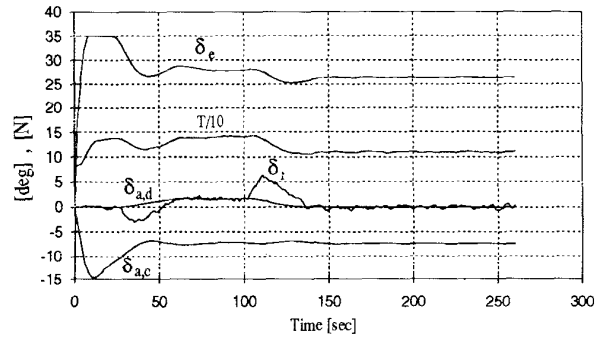

Figure 10: Control activity: Rudder (δ_r), Ailerons ($\delta_{a,c}$ and $\delta_{a,d}$), Elevator (δ_e) and Thruster (T).

At the beginning of the maneuver, the vehicle shows a pronounced rotation in pitch in order to converge rapidly to the desired vertical inclination of -10 deg. This rotation is achieved by deflecting the common rudder $\delta_{a,c}$ and

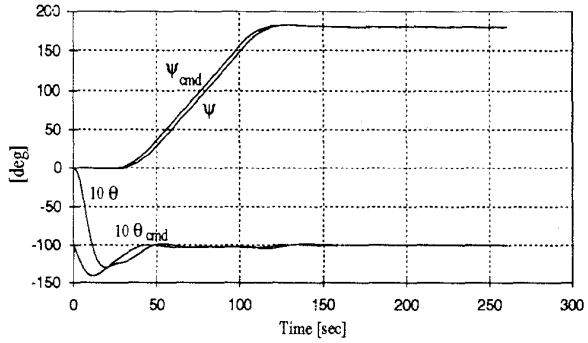

Figure 11: Commanded yaw (ψ_{cmd}) and pitch (θ_{cmd}) and respective measured angles.

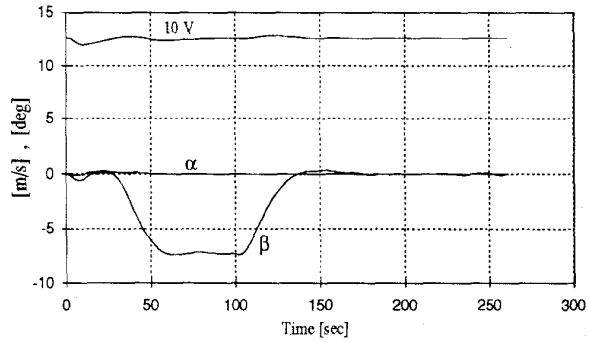

Figure 12: Velocity ($\mathbf{V}$), sideslip angle (β) and angle of attack (α).

the elevator δ_e in opposite directions, so as to generate a pure torque. During this phase, the elevator saturates. When the vehicle reaches the desired orientation, $\delta_{a,c}$ and δ_e decrease. However, their values don't tend to zero, since they must counteract the restoring torque due to the combined effects of buoyancy and gravity.

Upon entering the circular path, the rudder deflects to create a torque that will impart the desired rotational speed to the vehicle. Once the desired speed is reached, the rudder deflects slightly in the opposite direction to stabilize the rotation. This maneuver is characteristic of vehicles that are unstable in yaw. Finally, when the vehicle reaches the end of the circular path, there is a strong deflection in the rudder to drive the velocity of rotation to zero. During the final phase of the maneuver, the vehicle reaches an equilibrium condition with a pitch angle of -10 degrees.

It is important to remark that the thrust activity rises during maneuvers that require large deflection of the control surfaces. This is required to counteract the increase in drag, which tends to slow down the vehicle.

6 Conclusions

This paper has introduced an integrated approach to the design and analysis of guidance, navigation and control systems for AUVs. The methodology adopted has been applied to the design of a trajectory following system for the AUV MARIUS. Future work will address the problem of designing robust trajectory following systems to cope with large plant parameter uncertainty, as well as actuator and sensor failures.

References

[1] M. Abkowitz, "Lectures on Ship Hydrodynamics - Steering and Maneuverability," *report No. Hy-5, Hydrodynamics Department*, Technical University of Denmark, Lyngby, Denmark, May 1964.

[2] J. Bellingham, "Capabilities of Autonomous Underwater Vehicles," *Proceedings of the Workshop on Scientific and Environmental Data Collection with Autonomous Underwater Vehicles*, Cambridge,Massachusetts, US, March 1992, pp. 7-14.

[3] S. Boyd, V. Balakrishnan, and P. Kabamba,"On computing the $\mathcal{H}_\infty$ norm of a transfer matrix," *Mathematics of Control, Signals and Systems*, 1988.

[4] J. Craig, *Introduction to Robotics - Mechanics and Control*, Addison-Wesley, 1986.

[5] J. C. Doyle, K. Glover, P. P. Khargonekar, and B. A. Francis, "State space solutions to standard $\mathcal{H}_2$ and $\mathcal{H}_\infty$ control problems," *IEEE Transactions on Automatic Control*, AC-34(8), August 1989,pp. 831–847.

[6] P. Egeskov and A. Bjerrum, "Vehicle Design," *MARIUS-Technical Report*, COWIconsult, February 1994.

[7] P. Egeskov, A. Bjerrum, A. Pascoal, C. Silvestre, C. Aage and L. Wagner Smitt,"Design, Construction and Hydrodynamic Testing of the AUV MARIUS," *Proc. AUV 94*, Cambridge, Massachusetts, 1994.

[8] T. Fossen, *Nonlinear Modelling and Control of Underwater Vehicles*, doctoral dissertation, Norwegian Institute of Technology, 1991.

[9] G. Franklin, J. Powell and A. Emami-Naeini, *Feedback Control of Dynamic Systems*, Addison-Wesley Pub. Co., 1987.

[10] D. Fryxell, P. Oliveira, A. Pascoal and C. Silvestre "Modeling, Identification and Control of the AUV MARIUS," *SOUV-Technical Report*, Institute for Systems and Robotics, March 1994.

[11] D. Fryxell, *Modeling, Identification, Guidance and Control of an Autonomous Underwater Vehicle*, MSc Thesis, Department of Electrical Engineering, Instituto Superior Técnico, March 1994.

[12] Sv. Harvald, *Resistance and Propulsion of Ships*, JohnWiley and Sons, 1983.

[13] A. Healey and D. Lienard, "Multivariable sliding mode control for autonomous diving and steering of unmanned underwater vehicles," *IEEE Journal of Oceanic Engineering*, Vol. 18, N0.3, July 1993, pp. 327-339.

[14] E. Houghton and A. Brock, *Aerodynamics for Engineering Students*, Edward Arnold Pub. Ltd., 1977.

[15] B. Jacobi and A. Bjerrum, "Propulsion Test Planning, " *MARIUS-Technical Report*, COWIconsult, June 1992.

[16] I. Kaminer, A. M. Pascoal, P. P. Khargonekar, and C. Thomson,"A velocity algorithm for the implementation of gain-scheduled nonlinear controllers," *Proceedings of the second European Control Conference*, June 1993, pp. 787–792.

[17] I. Kaminer, A. M. Pascoal, C. Silvestre, and P. P. Khargonekar, "Design of a control system for an underwater vehicle using $\mathcal{H}_\infty$ synthesis," *Proceedings of the 30th Conference on Decision and Control*,December 1991.

[18] H. Lamb, *Hydrodynamics*, First Cambridge University Press, 1993.

[19] A. J. Laub."A Schur method for solving algebraic Riccati equations," *IEEE Transactions on Automatic Control*, AC-24(6), March 1979, pp. 913–921.

[20] C. Lin, *Modern Navigation, Guidance, and Control Processing*, Prentice-Hall, 1991.

[21] R. Meyer, and S. Burrus, "A unified analysis of multirate and periodically time-varying digital filters," *IEEE Transactions on Circuits and Systems*, CAS-22(3), March 1975, pp. 162–168.

[22] Axel Mølgaard, "PMM Tests with the Autonomous Underwater Vehicle MARIUS," *Technical Report No.1*, DMI 1152.92167, Danish Maritime Institute, March 1993.

[23] J. Newman, *Marine Hydrodynamics*, The MIT Press,1989.

[24] A. Pascoal, A. Bjerrum and J. Michel Coudeville, "MARIUS (Marine Utility System): An autonomous underwater vehicle for environmental surveying, " *Proceedings of the Mast Days and Euromar Market*, Commission of the European Communities, Brussels, Belgium, March 1993, pp. 746-758.

[25] A. Pascoal,"The AUV MARIUS: mission scenarios, vehicle design, construction and testing," *Proceedings of the 2nd Workshopon Mobile Robots for Subsea Environments*, Monterey Bay Aquarium, Monterey, California USA, May 1994.

[26] Fred Pucill, "Open Water Tests," *Technical Report No.1*, DMI 92060, Danish Maritime Institute , January 1993.

[27] C. Silvestre, *Modeling and Control of Autonomous Underwater Vehicles*, MSc Thesis, Instituto Superior Técnico, Lisbon, 1991.

[28] H. Sorenson, *Kalman Filtering: Theory and Application*, IEEE Press,1985.

[29] C. de Souza, "Periodic strong solution for the optimal filtering problem of linear discrete-time periodic systems," *IEEE Transactions on Automatic Control*, AC-36(3), March 1991, pp. 333–337.

[30] B. Stieler and H. Winter, *Gyroscopic Instruments and their Applications to Flight Testing*, AGARD Flight Test Intrumentation Series, AGARD, France, 1982.